Measuring a Cherenkov ring in the radio emission from air showers at 110-230 MHz with LOFAR

A. Nelles[a,b], P. Schellart[a], S. Buitink[a], A. Corstanje[a], J. E. Enriquez[a], H. Falcke[a,c,b,d], W. Frieswijk[c], J. R. Hörandel[a,b], O. Scholten[e], S. ter Veen[a], S. Thoudam[a], M. van den Akker[a], and the LOFAR Collaboration

[a] *Department of Astrophysics/IMAPP, Radboud University Nijmegen, P.O. Box 9010, 6500 GL Nijmegen, The Netherlands*
[b] *Nikhef, Science Park Amsterdam, 1098 XG Amsterdam, The Netherlands*
[c] *Netherlands Institute for Radio Astronomy (ASTRON), Postbus 2, 7990 AA Dwingeloo, The Netherlands*
[d] *Max-Planck-Institut für Radioastronomie, Auf dem Hügel 69, 53121 Bonn, Germany*
[e] *KVI, University Groningen, 9747 AA Groningen, The Netherlands*

Abstract

Measuring radio emission from air showers offers a novel way to determine properties of the primary cosmic rays such as their mass and energy. Theory predicts that relativistic time compression effects lead to a ring of amplified emission which starts to dominate the emission pattern for frequencies above $\sim 100\,\mathrm{MHz}$. The size of this ring is predicted to be sensitive to the atmospheric depth of the shower maximum, which in turn depends on the mass of the primary particle. In this article we present the first detailed measurements of this structure. Ring structures in the radio emission of air showers are measured with the LOFAR radio telescope in the frequency range of $110 - 230\,\mathrm{MHz}$. These data are well described by CoREAS simulations. They clearly confirm the importance of including the index of refraction of air as a function of height. Furthermore, the presence of the Cherenkov ring offers the possibility for a quick geometrical measurement of the depth of shower maximum.

Keywords: Cosmic rays, Extensive air showers, Radio emission, LOFAR, time-compression

1. Introduction

Since the discovery of radio emission from cosmic ray induced air showers in the 1960s [1, 2] it has been predicted that radio emission can be used as a tracer for arrival direction, mass, and energy of the primary particle. Experimentally it has been shown that the amplitude of the radio pulse scales with the energy of the primary particle [3]. Recently, it has also been demonstrated that the radio emission pattern observed at the ground is sensitive to the atmospheric depth of shower maximum $X_{\max}$ [4, 5]. This parameter which depends on the type or mass of the primary particle can be measured with an accuracy comparable to that of established techniques, such as the detection of Fluorescence or Cherenkov light (e.g.[6]), but with a much better duty cycle. Thus, it is possible to measure all important cosmic ray properties with radio detectors.

This progress would not have been made without thorough theoretical understanding of the emission processes. Recently, models describing the emission processes have converged to similar results [7]. The primary emission component is caused by deflection of charged leptons in the Earth's magnetic field, producing a coherent radio pulse that is polarized linearly in a direction perpendicular to the magnetic field direction and the direction of propagation of the air shower. A secondary component due to negative charge excess at the shower front also generates a coherent radio pulse that is polarized linearly, but now radially away from the shower axis. These components either add coherent or incoherently depending on the observer location, creating a complex emission pattern at ground level [8]. This pattern is further influenced by the non-constant and non-unity refractive index of the atmosphere, which leads to visible effects of relativistic time compression of the signal. Hereby emission is amplified for a specific angle with respect to the

shower axis [9, 10]. Since for the time compression the important measure is the size of the charged-particle distribution, millimetres in size, this effect is particularly strong at higher radio frequencies and allows shower emission to be detectable at GHz frequencies where coherence would otherwise be lost [11, 12].

The predicted observational signature of the relativistic time compression of the signal is a ring of amplified emission with a diameter in the order of 100 m, at the Cherenkov angle, therefore depending on the shower geometry [9]. For frequencies above 100 MHz this ring is predicted to dominate the emission pattern. From geometrical considerations it follows that the ring diameter should trace the distance to the shower maximum. This can be combined with atmospheric models to derive $X_{\max}$. Simulation studies confirm this basic idea [13]. Thus, measuring the ring diameter provides an alternate, air shower model independent, path to derive $X_{\max}$, which can be combined with air shower models to reconstruct the type of primary particle.

In this article, measurements of radio emission from cosmic ray air showers in the frequency range $110 - 230$ MHz are presented. While this frequency range has been probed inconclusively by several early experiments [1, 14, 15] and other recent experiments are also sensitive in this band [16], these data represent the first high-quality measurements of the radio pattern on a single event basis.

The instrument is described in section 2, followed by the employed data analysis techniques in section 3. The current dataset is characterized in section 4. Finally, in section 5 densely sampled signal patterns are shown and their implications for $X_{\max}$ measurements are discussed.

2. The instrument

LOFAR is a distributed radio telescope targeted at observing the lowest radio frequencies from 240 MHz down to the atmospheric cut-off at 10 MHz. The antennas of LOFAR are distributed over several European countries with a dense core in the Netherlands. The instrument was specifically designed to be able to observe short duration radio signals, such as those emitted by pulsars or cosmic ray induced air showers [17].

LOFAR covers the low frequency range with two types of antennas. The low-band antennas (*LBA*, $10 - 90$ MHz) consist of two inverted V-shaped dipole antennas, which are read-out individually. Their characteristics with respect to cosmic-ray air shower measurements are described in [18].

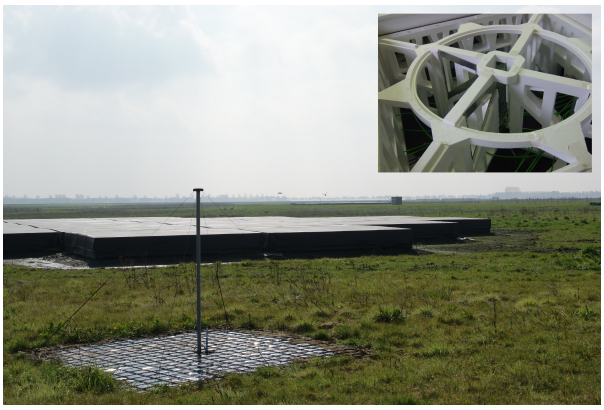

Figure 1: Radio antennas at LOFAR. Behind a low-band antenna a cluster of 24 black tiles of high-band antennas are shown. The inset shows the construction of a high-band element in which the bow-tie shaped antennas are mounted before they are packed in weather-proof foil.

The high-band antennas (*HBA*) cover the frequency range from $110 - 240$ MHz. In this range the antennas are no longer sky-noise dominated, which had to be accounted for in the design, while keeping the antennas as low cost as possible. One HBA *element* consist of dual-polarization fat dipole *antennas*, in which holes were cut to save material, making them similar to bow-tie antennas. The elements are arranged in a styrofoam structure and combined in groups of 16, called *tiles*. Every tile is packed in black foil, to protect the antenna electronics from the weather. Examples of an element and a tile can be seen in figure 1.

The HBA electronics have been optimized for targeted astronomical observations. The signals from all antennas in a tile are amplified and combined in an analog beamforming step. This means that the signals from the antennas are no longer available separately, but summed with a correction for a delay that a source from a certain direction would introduce. The delays to be applied are provided by the LOFAR control system for a user selectable direction. They are updated once every second to keep the direction of maximum sensitivity pointing in the same direction during an observation. A maximum delay of 17.7 ns can be introduced in 32 steps [19].

The HBAs (and LBAs) are grouped together in *stations* which themselves are distributed on a ir-

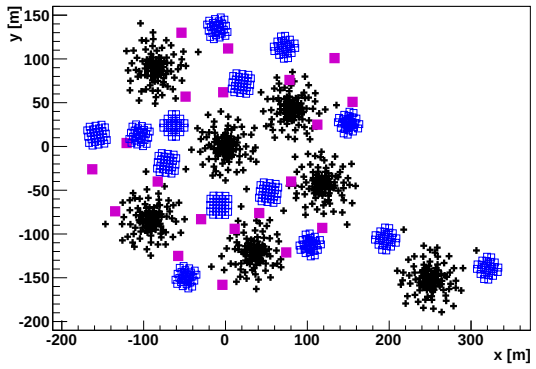

Figure 2: Central core of LOFAR. The black crosses are the low-band antennas, the blue open squares indicate the tiles of high-band antennas and the filled squares are the particle detectors.

regular grid to maximize the number of different baselines for interferometric observations. Near the center of LOFAR two groups of 24 tiles, called *sub-stations*, are associated with every station as indicated in figure 2. Further away from the core, 48 tiles in a single group belong to a station and international stations comprise a group of 96 tiles.

Parallel to an ongoing observation the tile-beamformed data from all HBA tiles are filled into ring buffers (Transient Buffer Boards), from which the last 5 s of data can be recorded when triggered. Triggers can be generated by inspecting the data with an on-board FPGA[1] or received through the LOFAR control software. In order to record cosmic-ray pulses, the dense core of LOFAR is equipped with an array of particle detectors [20], as also shown in figure 2. In routine observations, coincidences of several particle detectors trigger a read-out of the ring buffers.

The HBAs can be sampled at two different clock frequencies, which allows for several different observing bands. The one mostly used in the present data-set is $110 - 190$ MHz with 200 MHz sampling, i.e. second Nyquist zone. Alternatively, observations of $170 - 230$ MHz (160 MHz, third Nyquist zone) or $210 - 250$ MHz (200 MHz, third Nyquist zone) can be chosen. However, so far no cosmic-ray observations were conducted in the highest band.

[1]Field programmable gate array.

3. Detecting signals from cosmic rays

The detection of cosmic rays in the data from the HBAs is performed mostly analogous to that of the LBAs as described in [18]. Cosmic rays are detected in parallel to ongoing astronomical observation, which determines the direction of analogue beamforming. When a trigger from the array of particle detectors is received, the tile-beamformed data is written to disk and stored for processing. During processing, the signals from all tiles in a station are first coherently beamformed in the cosmic-ray arrival direction as reconstructed from the particle data. When a significant signal is detected in the beamformed signal the station is selected for further processing. Using a smaller search window, around the peak in the beamformed signal, a pulse search is then performed on the Hilbert envelope of the up-sampled signals from each tile. From the arrival times of the pulse maxima the direction of the cosmic ray is reconstructed. Additionally the amplitude (in each instrumental polarization) and integrated pulse power are extracted.

However, due to the different hardware and other dominant contributions to the background there are some differences in the reconstruction of the HBA data.

3.1. Removal of radio frequency interference (RFI)

The frequency band of the HBAs is less radio quiet than the LBA band. Especially an emergency pager signal at around 170 MHz adds a non-negligible amount of power to the spectrum. Therefore, before additional RFI removal is applied [18], all power in a band of 3 MHz around the pager frequency is set to zero with the edges convolved with a Gaussian to prevent artificial ringing in the signal.

Furthermore, single HBAs have been reported to occasionally show spikes in the data due to malfunctions. As such spikes will disturb the initial search for pulses in a beam formed trace, a simple spike search is performed after the RFI cleaning and antennas with spikes of outlying high amplitude are removed from the data-set.

3.2. Non-removable background

The HBAs are no longer fully dominated by the diffuse sky noise. In addition to the system noise, some astronomical sources introduce measurable signals in every single tile, most evident for bright sources such as Cas A or Cyg A. This means that the background noise in HBA observation is neither

uniform nor independent of the direction of observation.

With dedicated on- and off-source observations it was established that the noise-level will vary at most 15% due to different background sources, which reduces the sensitivity for cosmic ray observations. However, due to their brightness these sources are not a common target for HBA observations.

3.3. Gain corrections

The HBA antennas are not read out individually but rather in tile-groups of 16 antennas *after* analogue beamforming in the direction of the observation. In order to minimize artefacts in interferometric images, all individual HBA sub-stations are rotated at different unique angles (see section 2). While the antenna elements within a tile are counter rotated by the same amount in order to observe the same polarization component, the grid of 16 elements is oriented with the sub-station orientation. This gives a different tile sensitivity pattern for each HBA sub-station, resulting in different gains between sub-stations within one single cosmic-ray event.

To illustrate the complexities involved, figure 3 shows the influence of the analog tile-beamforming on a pure cosmic ray signal, without background noise, obtained from a CoREAS simulation. Here, the power gain

$$G_P = 10 \cdot \log_{10}\left(\frac{P_{\text{out}}}{P_{\text{in}}}\right) \quad (1)$$

is given as a function of the cosmic-ray arrival direction for two HBA sub-station orientations and two beam directions. The simplest pattern is obtained for a beam pointing towards zenith, where the delay corrections are zero and the signals from the individual antennas are simply added. The gain pattern is in this case solely the result of delays introduced by the arrival direction of the cosmic ray. However, for many LOFAR observations the beam is not pointing towards zenith, but rather towards some astronomical object. A frequently occurring pointing is towards the North Celestial Pole, which is given as a second example. While the beam shapes for tiles in two sub-stations look similar, there are significant differences as depicted in the bottom row of figure 3. These differences translate into differences in observed pulse amplitude of up to a factor of ~ 15 between tiles in two different sub-stations depending on the shower arrival direction. This means that while the beamforming always introduces an additional gain for cosmic rays arriving from the direction of the beam, the effect of the beamforming for off-beam cosmic rays will not be the same for every tile. While some signals might still be enhanced, others will be reduced to essentially noise-level.

The exact differences depend on the shape of the pulse and on the frequency response of the electronics. Furthermore, the complex direction and frequency dependent response pattern of the individual elements needs to be taken into account as well. Crosstalk between antenna elements, due to the close spacing within a tile, requires a response pattern per element as the patterns will be slightly different. Such a precise antenna model is still to be developed. Therefore, differences between tiles due to beamforming and antenna pattern are not corrected for in the present analysis.

In addition to the beam effect, there are intrinsic differences between stations and tiles. Gain differences between tiles within a station are corrected for using standard LOFAR calibration tables. These tables are generated regularly using the algorithms described in [21, 22]. The effect of possible gain differences between stations was tested, using data from the HBA part of the LOFAR MSSS survey [23]. The calibration values obtained form the pre-processed data of this survey vary between observations, but differ on average about 5% between stations in any given observation. As these values are not stable on longer time-scales, they are not used to correct for gain differences in this analysis. This introduces a 5% uncertainty on the pulse amplitudes measured in different stations.

4. Dataset

Cosmic-ray data have been gathered with the HBAs since October 2011. Until November 2013, 155 events have been detected in the band of $110 - 190\,\text{MHz}$ and two events in the band of $170 - 230\,\text{MHz}$. The time spent observing the lower of the two HBA bands was about 20 times longer.

The triggers from the scintillator array were sent according to the same specifications as for LBA observations [18]. These settings give a threshold energy of $2.4 \cdot 10^{16}\,\text{eV}$. While being recorded with the same trigger settings, the detection probability is roughly a factor two lower for HBA than for LBA. This difference can be attributed either to an intrinsically reduced emission strength at higher

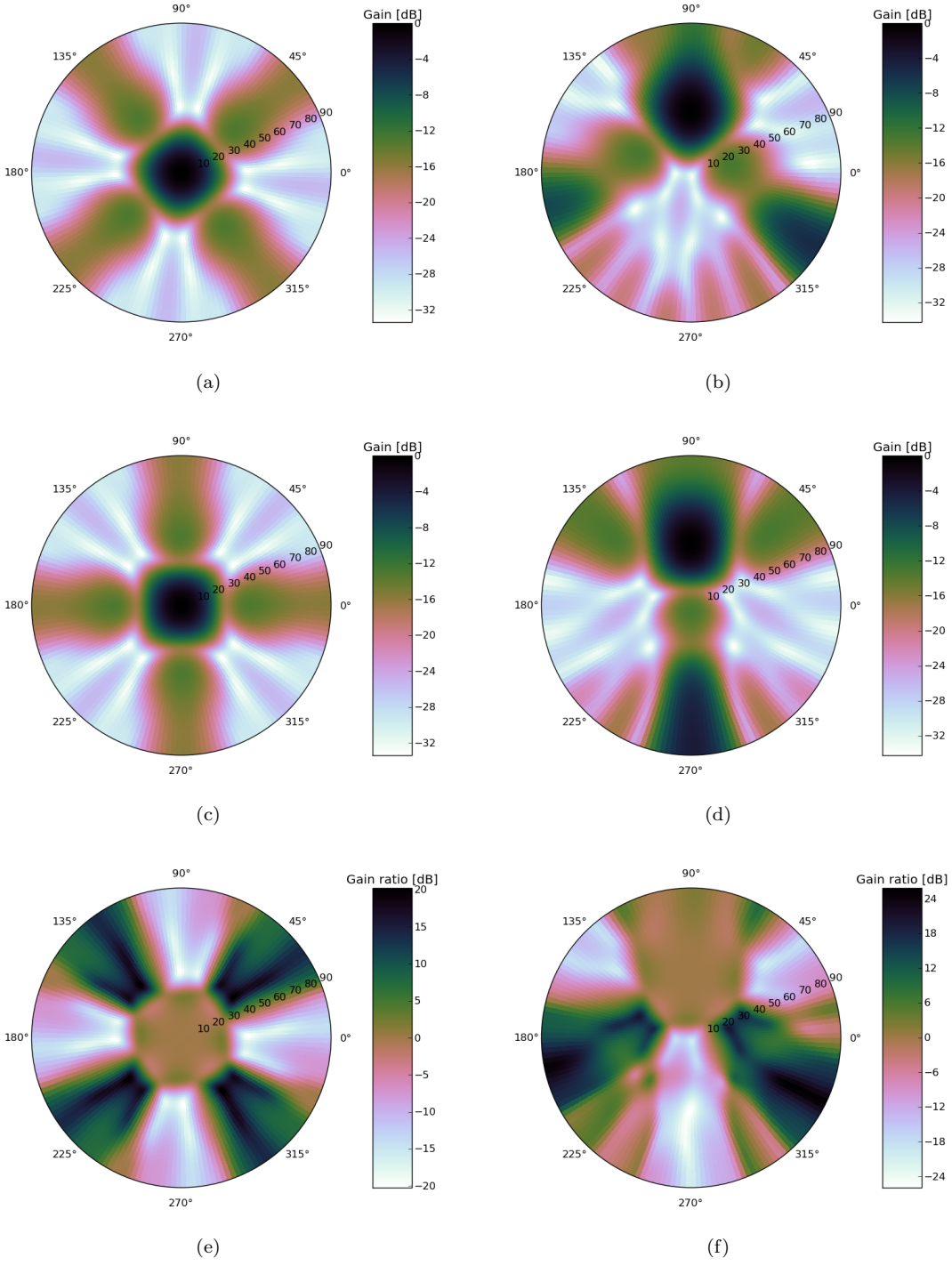

Figure 3: Influence of the tile-beamforming applied at the HBA tile-level. Shown is the resulting gain in power for tiles located in one of the two sub-stations making up an HBA core station for a beam pointing towards local zenith in figures (a), (c) and the North Celestial Pole in figures (b), (d). Figures (e) and (f) show the respective differences in gain between the two sub-stations. These differences result in offsets between the measured signal strength in different sub-stations depending on the shower arrival direction.

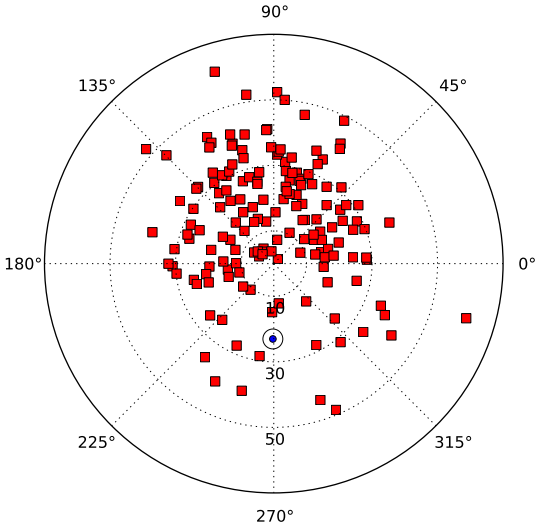

Figure 4: Directions of the detected cosmic rays on sky. 0° corresponds to west and 90° is north. The zenith angle ranges from 0° to 70°. Also indicated (blue circle) is the direction of the magnetic field at the LOFAR core, which is pointing downwards to north. A clear asymmetry of number of detected events is visible.

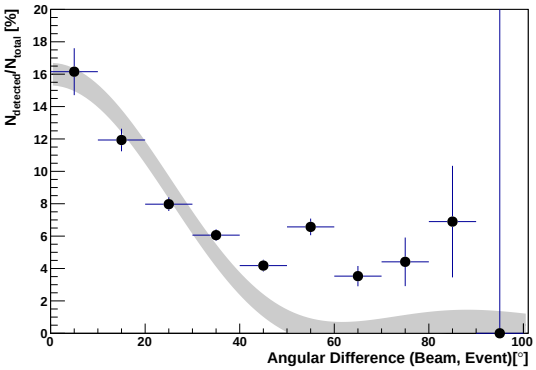

Figure 5: Probability of detecting an air shower as a function of angular difference between the direction of the observation and the arrival direction of the incoming cosmic ray. The grey contour shows a model of the extent of the beam-shape of an HBA tile. The model is scaled to match the cosmic ray data.

frequencies or instrumental effects such as higher background levels and hardware differences.

4.1. Information from particle data

Every triggered radio event is complemented with parameters reconstructed from the particle data. For every event two reconstructed directions are available, one from the particle data and one based on the radio signals. The angular resolution of the particle detectors is on average 1°. Further parameters obtainable from the particle data are the position of the shower axis and an energy estimate of the primary cosmic ray. Both parameters are only reliably reconstructed for a certain parameter space [18], and therefore not available for all events. The high quality events which are detected with the HBAs span an energy range from $1.7 \cdot 10^{16}$ eV to $1.1 \cdot 10^{18}$ eV.

4.2. Arrival directions

The arrival directions of the cosmic rays detected with the radio antennas are shown in figure 4. A clear north-south asymmetry is visible.

The angular resolution achieved with the HBA antennas is not the same for all directions. Many events are only measured with one station. As the antennas are clustered in two sub-stations, this results in a poorer angular resolution for showers arriving perpendicular to the axis connecting the two sub-stations. Also, the tile-beamforming has a negative effect on the accuracy as it affects the pulse shape and thereby influences the reconstruction of the arrival time. Thus, the cut applied in order to accept a trigger as cosmic-ray event is loosened with respect to the LBA data. An event is accepted when the directions reconstructed from particle data and radio agree within 20°, which is excludes in the current set only RFI events that can also be identified by their deviating pulse form.

4.3. Effect of the tile-beamforming

Due to the statistical nature of the cosmic ray arrival directions, no event arrived directly ($< 1°$) from the direction in which the beam of the observation was pointing.

The main effect of tile-beamforming in the direction of the shower is an increase in signal strength, which lowers the detection threshold. The main effect of beamforming in another direction than the arrival direction is a distortion of the pulse shape. This makes events of low signal strength harder to detect. Strong pulses are detectable, but the frequency content of the pulse as well as the position of the maximum will be affected. This effect is observed in data and visualized in figure 5, where the likelihood of detection is plotted as a function of angular distance between arrival direction and beam. The figure shows that events arriving closer to the

beam direction are more likely to be detected. Interesting to note is that the distribution roughly follows the predicted dimensions of the beam of the HBAs. Using the relation

$$G_{\mathrm{Beam}} \sim \frac{1}{\frac{\lambda}{D} \cdot \alpha} \cdot \sin\left(\frac{\lambda}{D} \cdot \alpha\right), \qquad (2)$$

with typical wavelength λ and detector size D, gives a full width half maximum beamwidth of about $\alpha = 20°$ for an HBA tile and the distribution shown in figure 5. This beamwidth also describes the regions depicted in figure 3, in which the gain is independent of the rotation of the sub-station. Both beam effects essentially limit the field of view and sensitivity for cosmic ray observations with the HBAs.

4.4. Observation of north-south asymmetry

The north-south asymmetry already pointed out in figure 4 has to be explained in the light of the effects of tile-beamforming. Figure 6 shows the distribution of the azimuth angles of the events and the directions of the relevant beams. The north-south asymmetry in the detection is clearly visible when comparing to the uniformity of the arrival direction of the air shower measured with the particle detectors, i.e. the triggers. This would clearly confirm the dominance of the geomagnetic effect, as the magnetic field is pointing directly north at LOFAR.

However, as figure 6 also shows, the observation beams were not uniformly distributed. Especially north is clearly preferred (north celestial pole). Therefore, an influence of the beam position cannot be excluded. However, as illustrated in table 1 there are significantly more detections from the northern half of the sky (c) than beams were pointed in this direction (b). Also, there is no significant selection effect of beams with a detection (b) from the whole set of beams (a). This means that the observed asymmetry cannot solely be explained by the distribution of beams. This is also illustrated by the second and fourth bin in figure 6. Despite very few beams having targeted these directions, there are a significant number of detections. A different explanation could be a bias due to observations which introduce high background levels, as described in section 3.2. However, even if all observations to the south targeted one of the bright sources, the additional background noise alone could not explain the asymmetry.

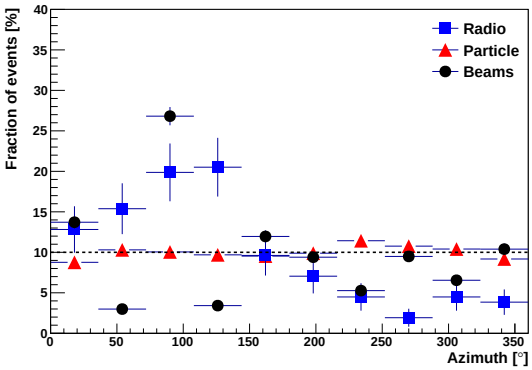

Figure 6: Distribution of arrival directions of the measured air showers with respect to azimuth angle. The azimuth angle is measured northwards positive from east. Shown are the different distributions of azimuth angles of the direction in which the data were tile-beamformed (black circles), the directions of the air showers that triggered LOFAR (red triangles) and the directions of the cosmic rays, which were detected in the radio (blue squares). The triggers are almost uniformly distributed while the beams of the astronomical observations and the radio detections are not.

	p(to/from north)
a: All beams	0.59 ± 0.01
b: Beams with detection	0.60 ± 0.04
c: Detected cosmic rays	0.78 ± 0.03
d: Not detected cosmic rays	0.48 ± 0.01

Table 1: Statistics concerning the distribution of azimuth angles of beam pointings and arrival directions. Probabilities are calculated for different scenarios to illustrate possible influences on the detection probability using the radio emission. For a uniform distribution $p = 0.5$ is expected for a cases. If the tile-beamforming was the only determining factor, p(c) should be compatible with p(a).

Thus, it can be concluded that also in this frequency range the geomagnetic effect plays a dominant role.

5. Observation of Cherenkov rings in air showers

The high antenna density of LOFAR enables detailed studies of the radiation pattern generated by individual showers. This is needed due to the intrinsic asymmetry of the signal which hinders averaging over showers. LOFAR is the only current experiment that can confirm theoretical predictions about the signal pattern in a single event study.

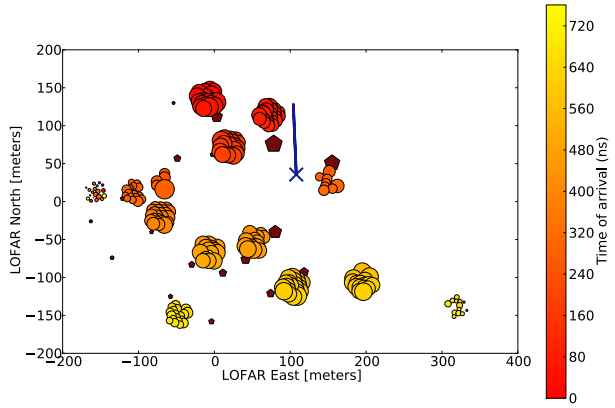

Figure 7: One air shower as measured with the HBAs. The dark red pentagrams depict the particle detectors. The colored circles represent the HBA tiles. In both cases, signal strength is encoded in the size of the markers. The arrival times of the radio pulses are encoded in the color of the circles going from early in red to late in yellow. The shower geometry as reconstructed from the particle data is shown with the blue cross and the line indicating the shower core and the projected arrival direction, respectively.

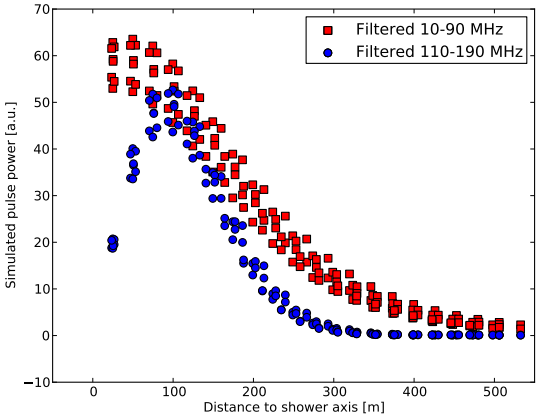

Figure 8: Simulated pulse power (CoReas) as a function of distance to shower axis for different ideal filter settings on an idealized grid of antennas. For this shower the primary particle was a proton of $7.2 \cdot 10^{17}$eV. As the pulse power is not a simple function of distance to shower axis, the spread represents the asymmetry in the signal.

5.1. Example event

Figure 7 shows an event as recorded with the HBAs. The distribution of signal strengths on the ground shows the detail and richness of features of the emission. It is however difficult to identify general structures by eye, given the irregular distribution of antennas and the projection of the radiation pattern from the shower plane onto the ground. Both will be accounted for when comparing the data to simulations.

5.2. Comparison to simulations

As shown in [4] the simulation code CoREAS [8] describes the data from the low-band antennas well and in great detail. With these simulations it can be illustrated what is expected from an observation at higher frequencies. Figure 8 shows the same simulations filtered in the two different LOFAR frequency bands. The shape of the lateral signal distribution changes and the ring like structure is more enhanced at higher frequencies, while the total power of the signal is decreasing with frequency.

A direct comparison of the HBA data using the method of [4] can only be accomplished under certain conditions. As discussed earlier, the additional gain differences of the HBA sub-stations according to their rotation make it challenging to correct for the hardware response. To do this correctly, one would have to simulate single pulses and feed them through a full model of the hardware, including especially the analogue beam former, which is very sensitive to uncertainties on the arrival direction. Such a realistic model of the full hardware is however not available yet.

Instead, we can concentrate on events that arrived from close to the direction of the beam. As shown in figures 3 and 5 the response of all HBA sub-stations is similar for events arriving from the full-width-half-maximum (FWHM) of the main beam. We therefore selected three events arriving with the FWHM of the initial beam direction with more than four triggered stations and compared them to simulations. All three events arrived from close to the north celestial pole and can be reproduced by simulations. The best fitting simulations for the three events are shown in figure 9. In the images on the left-hand side, the interpolated total power from the simulation is given in the background map. Overlaid are the measured data as circles. Where the colors match there is an agreement in signal strength. The Cherenkov ring clearly dominates the structure for all events in both simulations and measurements.

The same can be seen in a projection of the signals as a function of distance to shower axis as shown on the right-hand side of figure 9. This lateral distribution is clearly dominated by the am-

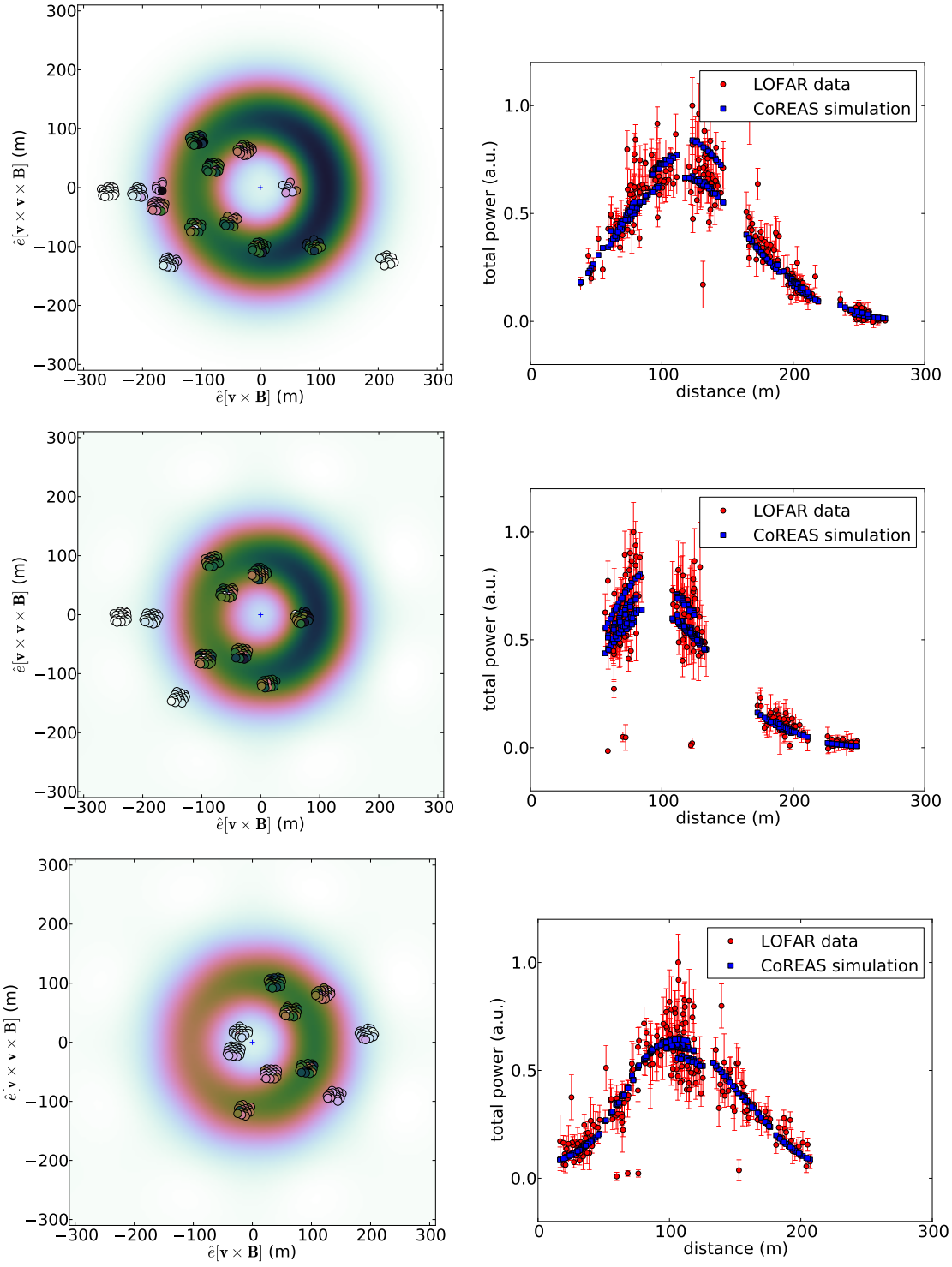

Figure 9: Comparison of measurements and simulations for three air showers. Left: Signal distribution in shower plane. The circles indicate the positions of the signal measurements. The background map is the interpolated signal strength from the best fitting simulated CoREAS shower. The integrated power from $110 - 190$ MHz both for measurements and simulations is encoded in color. The reference coordinate system is the shower plane defined by the propagation vector $\mathbf{v}$ and magnetic field direction $\mathbf{B}$. The shower axis is located at the plus sign. Right: Corresponding integrated radio pulse power for simulation (blue squares) and LOFAR HBA measurements (red circles) as a function of distance to shower axis.

plified ring structure at distances of about 100 meters. These measurements clearly confirm the importance of the propagation of the radiation, which causes these relativistic time compression of the measured emission, which itself is still dominated by the geomagnetic effect (see 4.4).

5.3. Sensitivity of the Cherenkov ring to the depth of the shower maximum

It was suggested in [13] that the radius of the Cherenkov ring is sensitive to the depth of shower maximum $X_{\max}$. With a precisely obtained radius a resolution of $10-15\,\mathrm{g/cm^2}$ is achievable for vertical showers. Experimentally, it has to be tested how accurately the radius of the ring can be measured and what resolution this yields for $X_{\max}$.

The three events introduced above are used to determine the accuracy with which the radius of the Cherenkov ring is obtained. The main contribution to the overall uncertainty is the uncertainty on the position of the shower axis. Unless there is a complete fit of the signal distribution of the radio data, the axis as obtained by the particle array has to be used. These uncertainties differ for each event and vary from 5 meters to 30 meters.

Another contribution to the overall uncertainty is the one on the model which is used to fit the radius of the ring. As there is still some asymmetry visible in the emission pattern, a one-dimensional fit to describe the whole distribution is not sufficient. It seems, however, that the radius of the ring is sufficiently symmetric in the shower plane to approximate this feature in one dimension. Given the uncertainties on the signals and using the results of earlier observations that the fall-off of the signal can be approximated by an exponential function [24], a fit of a Gaussian function, centred on the ring, is chosen. This approach, however, introduces additional uncertainties.

A last non-negligible factor is the arrival direction of the shower. Since most of the ring size can be attributed to the propagation of the shower in the atmosphere, the pathlength on which the shower develops is essential, which in turn is a function of inclination angle. The parameters reconstructed from the radio data [18] for the three example showers are shown in table 2.

In [13] $X_{\max}$ is calculated by fitting the following relation to a set of air showers, simulated using the EVA code [25], with energies between $10^{17}-10^{19}\,\mathrm{eV}$ of vertical arrival direction:

$$X_{\max} = a + b \cdot d_p. \tag{3}$$

Here a and b are fitted constants and d_p describes the radius of the ring. The same analysis was repeated for showers of more horizontal arrival directions (30° and 45°) in the frequency range of $110-190\,\mathrm{MHz}$ [26]. For a perfectly measured radius of the ring a resolution of better than $30\,\mathrm{g/cm^2}$ is achieved for vertical showers. The method gets less precise for inclined showers. Adding the additional uncertainties for the reconstruction of the ring, yields the results as shown in table 3. The results are compared to the best fit obtained from simulating several air showers using CoReas with different $X_{\max}$ for a single event (see [4]). The latter value is given for reference purposes and cannot be used to compare the two models (EVA and CoReas), as two completely different methods are applied to obtain $X_{\max}$.

The results show that there is, given the three events, no statistically significant discrepancy between the two methods. The large uncertainties obtained for $X_{\max}$, determined through the ring size, prevents more precise statements.

There are a number of additional uncertainties that need to be considered for comparing the results. As shown in [13] the frequency range in which the shower is measured has a strong effect on the location of the ring. As there is no full antenna model to correct the HBA observations to a fully flat frequency spectrum, this might bias the results. Also,

Event	Zenith angle [°]	Radius of ring [m]
1	43.4 ± 2.0	117.3 ± 4.7
2	34.9 ± 1.0	93.3 ± 2.1
3	40.5 ± 1.0	119.6 ± 22.1

Table 2: Shower parameters determining the measurement of $X_{\max}$. The angle is measured from zenith (upwards: 0°) and reconstructed from radio data. The ring size is determined according to the procedure described in section 5.3.

Event	Fit: $X_{\max}$ [g/cm^2]	Sim: $X_{\max}$ [g/cm^2]
1	$45° : 612 \pm 88$	675 ± 22
2	$30° : 538 \pm 58$	643 ± 27
3	$45° : 595 \pm 156$	671 ± 37

Table 3: The height of the shower maximum $X_{\max}$ as obtained for the example events. The methods are using a parametrization for different zenith angles (Fit) or dedicated individual simulations (Sim).

the missing antenna correction influences the $X_{\max}$ obtained with direct comparison of simulations, as the hardware response could not be included in the analysis as it is done for measurements with the low-band antennas. It also should be noted that there is no parametrization as a function of zenith angle yet and the events are approximated by the closest available parametrization.

We show that the radius of the Cherenkov ring can be used with experimental data as an indicator for the depth of the shower maximum. However, the obtainable accuracy is far less than needed for a precise composition study. It is therefore necessary to use more information than just the ring size. The distribution of the signal is a non-symmetric function of several shower parameters, which calls for a more complex fitting procedure or a direct comparison to simulated showers [4]. Possible discrepancies between models of the radio emission of air showers are not tested by this analysis.

6. Conclusions and Outlook

The data of air showers collected with the LOFAR high-band antennas provide unprecedented detailed measurements of radio emission in the frequency range of $110 - 230\,\mathrm{MHz}$. In standard observation mode, 157 cosmic rays were measured since October 2011.

The HBAs were designed to observe (astronomical) objects in pre-defined directions. The effect of the analogue beamforming is difficult to remove completely for cosmic-ray measurements. It influences the absolute calibration between groups of HBA antennas and affects the shape of the pulses. However, we show that it is worthwhile to attempt a detailed correction of the hardware effects.

For the first time, we measure a dominant relativistic time compression of the radio emission of air showers on a single-event basis. We show that it is possible to measure the radius of this Cherenkov ring with an accuracy of less than 20 meters. This is sufficient to give an indication of the depth of shower maximum. However, more complex procedures are needed to resolve the shower maximum with the necessary accuracy for composition studies. Given that LOFAR is observing at $110 - 230\,\mathrm{MHz}$ roughly 50% of the time, reconstructing the HBA data to a better quality will significantly increase the event statistics for composition studies at LOFAR.

Also, measuring the same air shower with both types of antennas is very promising. The well-understood measurements with the LBAs could be extended to higher frequencies to learn more about the emission mechanisms. The current measurements strongly encourage to implement this mode of combined observation in the complete frequency range from $10 - 240\,\mathrm{MHz}$ in LOFAR.

Acknowledgements

The authors would like to thank K. de Vries for providing an update to his published analysis. The LOFAR cosmic ray key science project very much acknowledges the scientific and technical support from ASTRON. Furthermore, we acknowledge financial support from the Netherlands Research School for Astronomy (NOVA), the Samenwerkingsverband Noord-Nederland (SNN), the Foundation for Fundamental Research on Matter (FOM) and the Netherlands Organization for Scientific Research (NWO), VENI grant 639-041-130. We acknowledge funding from an Advanced Grant of the European Research Council under the European Unions Seventh Framework Program (FP/2007-2013) / ERC Grant Agreement n. 227610.

LOFAR, the Low Frequency Array designed and constructed by ASTRON, has facilities in several countries, that are owned by various parties (each with their own funding sources), and that are collectively operated by the International LOFAR Telescope (ILT) foundation under a joint scientific policy.

References

[1] J. V. Jelley, W. N. Charman, J. H. Fruin, F. Graham Smith, R. A. Porter, N. A. Porter, T. C. Weekes, B. McBreen, Radio pulses from extensive air showers, Il Nuovo Ciemento A 46 (4) (1966) 649–667. doi:10.1007/BF02857512.

[2] H. Allan, J. Jones, Radio Pulses from Extensive Air Showers, Nature 212 (1966) 129–131. doi:10.1038/212129a0.

[3] H. Falcke, W. D. Apel, A. F. Badea, L. Bähren, K. Bekk, A. Bercuci, M. Bertaina, P. L. Biermann, J. Blümer, H. Bozdog, I. M. Brancus, S. Buitink, M. Brüggemann, P. Buchholz, H. Butcher, A. Chiavassa, K. Daumiller, A. G. de Bruyn, C. M. de Vos, F. di Pierro, P. Doll, R. Engel, H. Gemmeke, P. L. Ghia, R. Glasstetter, C. Grupen, A. Haungs, D. Heck, J. R. Hörandel, A. Horneffer, T. Huege, K.-H. Kampert, G. W. Kant, U. Klein, Y. Kolotaev, Y. Koopman, O. Krömer, J. Kuijpers, S. Lafebre, G. Maier, H. J. Mathes, H. J. Mayer, J. Milke, B. Mitrica,

C. Morello, G. Navarra, S. Nehls, A. Nigl, R. Obenland, J. Oehlschläger, S. Ostapchenko, S. Over, H. J. Pepping, M. Petcu, J. Petrovic, S. Plewnia, H. Rebel, A. Risse, M. Roth, H. Schieler, G. Schoonderbeek, O. Sima, M. Stümpert, G. Toma, G. C. Trinchero, H. Ulrich, S. Valchierotti, J. van Buren, W. van Cappellen, W. Walkowiak, A. Weindl, S. Wijnholds, J. Wochele, J. Zabierowski, J. A. Zensus, D. Zimmermann, Detection and imaging of atmospheric radio flashes from cosmic ray air showers, Nature 435 (2005) 313–316. arXiv:arXiv:astro-ph/0505383, doi:10.1038/nature03614.

[4] S. Buitink for the LOFAR Collaboration, Shower Xmax determination based on LOFAR radio measurements), year = 2013, in: Proceedings of the 33rd International Cosmic Ray Conference.

[5] W. D. Apel, J. C. Arteaga, L. Bähren, K. Bekk, M. Bertaina, P. L. Biermann, J. Blümer, H. Bozdog, I. M. Brancus, P. Buchholz, E. Cantoni, A. Chiavassa, K. Daumiller, V. de Souza, F. Di Pierro, P. Doll, R. Engel, H. Falcke, M. Finger, B. Fuchs, D. Fuhrmann, H. Gemmeke, C. Grupen, A. Haungs, D. Heck, J. R. Hörandel, A. Horneffer, D. Huber, T. Huege, P. G. Isar, K.-H. Kampert, D. Kang, O. Krömer, J. Kuijpers, K. Link, P. Łuczak, M. Ludwig, H. J. Mathes, M. Melissas, C. Morello, J. Oehlschläger, N. Palmieri, T. Pierog, J. Rautenberg, H. Rebel, M. Roth, C. Rühle, A. Saftoiu, H. Schieler, A. Schmidt, F. G. Schröder, O. Sima, G. Toma, G. C. Trinchero, A. Weindl, J. Wochele, M. Wommer, J. Zabierowski, J. A. Zensus, Experimental evidence for the sensitivity of the air-shower radio signal to the longitudinal shower development, Phys. Rev. D 85 (2012) 071101. doi:10.1103/PhysRevD.85.071101.

[6] K.-H. Kampert, M. Unger, Measurements of the cosmic ray composition with air shower experiments, Astroparticle Physics 35 (2012) 660–678. doi:10.1016/j.astropartphys.2012.02.004.

[7] T. Huege, M. Ludwig, O. Scholten, K. D. de Vries, The convergence of EAS radio emission models and a detailed comparison of REAS3 and MGMR simulations, Nuclear Instruments and Methods in Physics Research A 662 (2012) 179. doi:10.1016/j.nima.2010.11.041.

[8] T. Huege, M. Ludwig, C. W. James, Simulating radio emission from air showers with coreas, ARENA 2012, AIP Conf. Proc. 1535 (2013) 128–132doi:http://dx.doi.org/10.1063/1.4807534.

[9] K. D. de Vries, A. M. van den Berg, O. Scholten, K. Werner, Coherent cherenkov radiation from cosmic-ray-induced air showers, Phys. Rev. Lett. 107 (2011) 061101. doi:10.1103/PhysRevLett.107.061101.

[10] J. Alvarez-Muñiz, W. R. Carvalho, Jr., A. Romero-Wolf, M. Tueros, E. Zas, Coherent radiation from extensive air showers in the ultrahigh frequency band, Phys Rev. D86 (12) (2012) 123007. arXiv:1208.0951, doi:10.1103/PhysRevD.86.123007.

[11] S. Hoover, J. Nam, P. W. Gorham, E. Grashorn, P. Allison, S. W. Barwick, J. J. Beatty, K. Belov, D. Z. Besson, W. R. Binns, C. Chen, P. Chen, J. M. Clem, A. Connolly, P. F. Dowkontt, M. A. DuVernois, R. C. Field, D. Goldstein, A. G. Vieregg, C. Hast, M. H. Israel, A. Javaid, J. Kowalski, J. G. Learned, K. M. Liewer, J. T. Link, E. Lusczek, S. Matsuno, B. C. Mercurio, C. Miki, P. Miočinović, C. J. Naudet, J. Ng, R. J. Nichol, K. Palladino, K. Reil, A. Romero-Wolf, M. Rosen, L. Ruckman, D. Saltzberg, D. Seckel, G. S. Varner, D. Walz, F. Wu, Observation of ultrahigh-energy cosmic rays with the anita balloon-borne radio interferometer, Phys. Rev. Lett. 105 (2010) 151101. doi:10.1103/PhysRevLett.105.151101.

[12] R. Smida, F. Werner, R. Engel, J. C. Arteaga-Velazquez, K. Bekk, M. Bertaina, J. Bluemer, H. Bozdog, I. M. Brancus, A. Chiavassa, F. Cossavella, F. Di Pierro, P. Doll, B. Fuchs, D. Fuhrmann, C. Grupen, A. Haungs, D. Heck, J. R. Hoerandel, D. Huber, T. Huege, K.-H. Kampert, D. Kang, H. Klages, M. Kleifges, O. Kroemer, K. Link, P. Luczak, M. Ludwig, H. J. Mathes, H. J. Mayer, S. Mathys, M. Melissas, C. Morello, P. Neunteufel, J. Oehlschlaeger, N. Palmieri, J. Pekala, T. Pierog, J. Rautenberg, H. Rebel, M. Riegel, M. Roth, F. Salamida, H. Schieler, S. Schoo, F. G. Schroeder, O. Sima, J. Stasielak, G. Toma, G. C. Trinchero, M. Unger, M. Weber, A. Weindl, H. Wilczynski, M. Will, J. Wochele, J. Zabierowski, Observation of Polarised Microwave Emission from Cosmic Ray Air Showers, in: 33rd International Cosmic Ray Conference, ICRC Rio de Janiero, 2013.

[13] K. D. de Vries, O. Scholten, K. Werner, The air shower maximum probed by Cherenkov effects from radio emission, Astroparticle Physics 45 (2013) 23–27. arXiv:1304.1321, doi:10.1016/j.astropartphys.2013.02.003.

[14] W. Charman, J. Jelley, A search at the zenith for 200 mhz and 3000 mhz radio emission from extensive air showers, Il Nuovo Cimento 63B (2) (1969) 473–485. doi:10.1007/BF02710700.

[15] R. Spencer, Radio Pulses from Cosmic Ray Air Showers at 44, 105, 239 and 408 MHz, Nature 222 (1969) 460–461. doi:10.1038/222460a0.

[16] D. Ardouin, A. Belletoile, C. Berat, D. Breton, D. Charrier, J. Chauvin, M. Chendeb, A. Cordier, S. Dagoret-Campagne, R. Dallier, L. Denis, C. Dumez-Viou, C. Fabrice, T. Garçon, X. Garrido, N. Gautherot, T. Gousset, F. Haddad, D. H. Koang, J. Lamblin, P. Lautridou, D. Lebrun, A. Lecacheux, F. Lefeuvre, L. Martin, E. Meyer, F. Meyer, N. Meyer-Vernet, D. Monnier-Ragaigne, F. Montanet, K. Payet, G. Plantier, O. Ravel, B. Revenu, C. Riviere, T. Saugrin, A. Sourice, P. Stassi, A. Stutz, S. Valcares, Geomagnetic origin of the radio emission from cosmic ray induced air showers observed by CODALEMA, Astroparticle Physics 31 (2009) 192–200. doi:10.1016/j.astropartphys.2009.01.001.

[17] M. P. van Haarlem, M. W. Wise, A. W. Gunst, G. Heald, J. P. McKean, J. W. T. Hessels, A. G. de Bruyn, R. Nijboer, J. Swinbank, R. Fallows, M. Brentjens, A. Nelles, R. Beck, H. Falcke, R. Fender, J. Hörandel, L. V. E. Koopmans, G. Mann, G. Miley, H. Röttgering, B. W. Stappers, R. A. M. J. Wijers, S. Zaroubi, M. van den Akker, A. Alexov, J. Anderson, K. Anderson, A. van Ardenne, M. Arts, A. Asgekar, I. M. Avruch, F. Batejat, L. Bähren, M. E. Bell, M. R. Bell, I. van Bemmel, P. Bennema, M. J. Bentum, G. Bernardi, P. Best, L. Bîrzan, A. Bonafede, A.-J. Boonstra, R. Braun, J. Bregman, F. Breitling, R. H. van de Brink, J. Broderick, P. C. Broekema, W. N. Brouw, M. Brüggen, H. R. Butcher, W. van Cappellen, B. Ciardi, T. Coenen, J. Conway, A. Coolen, A. Corstanje, S. Damstra, O. Davies, A. T. Deller, R.-J. Dettmar,

G. van Diepen, K. Dijkstra, P. Donker, A. Doorduin, J. Dromer, M. Drost, A. van Duin, J. Eislöffel, J. van Enst, C. Ferrari, W. Frieswijk, H. Gankema, M. A. Garrett, F. de Gasperin, M. Gerbers, E. de Geus, J.-M. Grießmeier, T. Grit, P. Gruppen, J. P. Hamaker, T. Hassall, M. Hoeft, H. A. Holties, A. Horneffer, A. van der Horst, A. van Houwelingen, A. Huijgen, M. Iacobelli, H. Intema, N. Jackson, V. Jelic, A. de Jong, E. Juette, D. Kant, A. Karastergiou, A. Koers, H. Kollen, V. I. Kondratiev, E. Kooistra, Y. Koopman, A. Koster, M. Kuniyoshi, M. Kramer, G. Kuper, P. Lambropoulos, C. Law, J. van Leeuwen, J. Lemaitre, M. Loose, P. Maat, G. Macario, S. Markoff, J. Masters, R. A. McFadden, D. McKay-Bukowski, H. Meijering, H. Meulman, M. Mevius, E. Middelberg, R. Millenaar, J. C. A. Miller-Jones, R. N. Mohan, J. D. Mol, J. Morawietz, R. Morganti, D. D. Mulcahy, E. Mulder, H. Munk, L. Nieuwenhuis, R. van Nieuwpoort, J. E. Noordam, M. Norden, A. Noutsos, A. R. Offringa, H. Olofsson, A. Omar, E. Orrú, R. Overeem, H. Paas, M. Pandey-Pommier, V. N. Pandey, R. Pizzo, A. Polatidis, D. Rafferty, S. Rawlings, W. Reich, J.-P. de Reijer, J. Reitsma, G. A. Renting, P. Riemers, E. Rol, J. W. Romein, J. Roosjen, M. Ruiter, A. Scaife, K. van der Schaaf, B. Scheers, P. Schellart, A. Schoenmakers, G. Schoonderbeek, M. Serylak, A. Shulevski, J. Sluman, O. Smirnov, C. Sobey, H. Spreeuw, M. Steinmetz, C. G. M. Sterks, H.-J. Stiepel, K. Stuurwold, M. Tagger, Y. Tang, C. Tasse, I. Thomas, S. Thoudam, M. C. Toribio, B. van der Tol, O. Usov, M. van Veelen, A.-J. van der Veen, S. ter Veen, J. P. W. Verbiest, R. Vermeulen, N. Vermaas, C. Vocks, C. Vogt, M. de Vos, E. van der Wal, R. van Weeren, H. Weggemans, P. Weltevrede, S. White, S. J. Wijnholds, T. Wilhelmsson, O. Wucknitz, S. Yatawatta, P. Zarka, A. Zensus, J. van Zwieten, LOFAR: The LOw-Frequency ARray, Astronomy and Astrophysics 556 (2013) A2. arXiv:1305.3550, doi:10.1051/0004-6361/201220873.

[18] P. Schellart, A. Nelles, S. Buitink, A. Corstanje, J. E. Enriquez, H. Falcke, W. Frieswijk, J. R. Hörandel, A. Horneffer, C. W. James, M. Krause, M. Mevius, O. Scholten, S. ter Veen, S. Thoudam, M. van den Akker, A. Alexov, J. A. andI. M. Avruch, L. Bähren, R. Beck, M. E. Bell, P. Bennema, M. J. Bentum, G. Bernardi, P. Best, J. Bregman, F. Breitling, M. Brentjens, J. Broderick, M. Brüggen, B. Ciardi, A. Coolen, F. de Gasperin, E. de Geus, A. de Jong, M. de Vos, S. Duscha, J. Eislöffel, R. A. Fallows, C. Ferrari, M. A. Garrett, J. Griessmeier, T. Grit, J. P. Hamaker, T. E. Hassall, G. Heald, J. W. T. Hessels, M. Hoeft, H. A. Holties, M. Iacobelli, E. Juette, A. Karastergiou, W. Klijn, J. Kohler, V. I. Kondratiev, M. Kramer, M. Kuniyoshi, G. Kuper, P. Maat, G. Macario, G. Mann, S. Markoff, D. McKay-Bukowski, J. P. McKean, J. C. A. Miller-Jones, D. D. M. J. D. Mol and, H. M. andR. Nijboer, M. J. Norden, E. Orru3, R. Overeem, H. Paas, M. Pandey-Pommier, R. Pizzo, A. G. Polatidis, A. Renting, J. W. Romein, H. Röttgering, A. Schoenmakers, D. Schwarz, J. Sluman, O. Smirnov, C. Sobey, B. W. Stappers, M. Steinmetz, J. Swinbank, Y. Tang, C. Tasse, C. Toribio, J. van Leeuwen, R. van Nieuwpoort, R. J. van Weeren, N. Vermaas, R. Vermeulen, C. Vocks, C. Vogt, R. A. M. J. Wijers, S. J. Wijnholds, M. W. Wise, O. Wucknitz, S. Yatawatta, P. Zarka, , A. Zensus, Detecting cosmic rays with the lofar radio telescope, A&A 560 (2013) A98. doi:10.1051/0004-6361/201322683.

[19] G. Kant, A. Gunst, M. Drost, High band antenna – architectual design document, Tech. rep., ASTRON (2007).

[20] S. Thoudam, S. Buitink, A. Corstanje, J. E. Enriquez, H. Falcke, W. Frieswijk, J. R. Hörandel, A. Horneffer, C. W. James, M. Krause, M. Mevius, A. Nelles, P. Schellart, O. Scholten, S. ter Veen, S. Thoudam, M. van den Akker, The LOFAR Collaboration, Lora: A scintillator array for lofar to measure extensive air showers, submitted for publication in Nucl. Instr. Meth. (2014).

[21] S. J. Wijnholds, A.-J. van der Veen, Multisource Self-Calibration for Sensor Arrays, IEEE Transactions on Signal Processing 57 (2009) 3512–3522. arXiv:1003.1892, doi:10.1109/TSP.2009.2022894.

[22] S. J. Wijnholds, A.-J. van der Veen, Self-Calibration of Radio Astronomical Arrays With Non-Diagonal Noise Covariance Matrix, ArXiv e-printsarXiv:1003.2497.

[23] G. Heald, LOFAR Collaboration, The LOFAR Multifrequency Snapshot Sky Survey (MSSS): Status and Results, in: American Astronomical Society Meeting Abstracts, Vol. 221 of American Astronomical Society Meeting Abstracts, 2013, p. 215.07.

[24] W. D. Apel, J. C. Arteaga, T. Asch, A. F. Badea, L. Bähren, K. Bekk, M. Bertaina, P. L. Biermann, J. Blümer, H. Bozdog, I. M. Brancus, M. Brüggemann, P. Buchholz, S. Buitink, E. Cantoni, A. Chiavassa, F. Cossavella, K. Daumiller, V. de Souza, F. di Pierro, P. Doll, R. Engel, H. Falcke, M. Finger, D. Fuhrmann, H. Gemmeke, P. L. Ghia, R. Glasstetter, C. Grupen, A. Haungs, D. Heck, J. R. Hörandel, A. Horneffer, T. Huege, P. G. Isar, K.-H. Kampert, D. Kang, D. Kickelbick, O. Krömer, J. Kuijpers, S. Lafebre, P. Łuczak, M. Ludwig, H. J. Mathes, H. J. Mayer, M. Melissas, B. Mitrica, C. Morello, G. Navarra, S. Nehls, A. Nigl, J. Oehlschläger, S. Over, N. Palmieri, M. Petcu, T. Pierog, J. Rautenberg, H. Rebel, M. Roth, A. Saftoiu, H. Schieler, A. Schmidt, F. Schröder, O. Sima, K. Singh, G. Toma, G. C. Trinchero, H. Ulrich, A. Weindl, J. Wochele, M. Wommer, J. Zabierowski, J. A. Zensus, LOPES Collaboration, Lateral distribution of the radio signal in extensive air showers measured with LOPES, Astroparticle Physics 32 (2010) 294–303. doi:10.1016/j.astropartphys.2009.09.007.

[25] K. Werner, K. D. de Vries, O. Scholten, A realistic treatment of geomagnetic Cherenkov radiation from cosmic ray air showers, Astroparticle Physics 37 (2012) 5–16. arXiv:1201.4471, doi:10.1016/j.astropartphys.2012.07.007.

[26] K. D. de Vries, private communication.